REVISTA MATÉRIA
V.25 N.01
ISSN 1517-7076 articles e-12601, 2020

Effect of HA Nanoparticles on Adsorption of Vitamin D3 on Super-Hydrophobic PA6 Nanofibrous Scaffold

Hamid Esfahani [1], Yasaman Ghiyasi [1]

[1] Department of Materials Engineering, 65178-38695, Bu-Ali Sina University, Hamedan, Hamedan, Iran.
e-mail: h.esfahani@basu.ac.ir

ABSTRACT

Vitamin D_3 has significant roles in bone growth and the prevention of osteoporotic fractures. The present study investigated the effect of hydroxyapatite nanoparticles decoration onto polyamide-6 nanofibrous scaffold on adsorption behaviour of Vitamin D_3. To synthesize the nanofibrous scaffold, an electrospinning device was used, and the surface of the scaffold was characterized by scanning electron microscopy, energy dispersive spectrometry, Fourier transform infrared spectroscopy, and measurement of the water contact angle. The antibacterial activity test against *E. coli* and *S. aureus* bacteria indicated no such activity of pristine and hydroxyapatite decorated scaffold. The results demonstrated that a hydrophobic and high porous scaffold was formed, and hydroxyapatite nanoparticles were distributed inside the polyamide-6 nanofibers homogenously. Results showed that the hydroxyapatite nanoparticles improved the adsorption efficiency of polyamide-6 scaffold. It was found that the amount of adsorbed Vitamin D_3 molecules onto the polyamide-6/HA scaffold was rapid during the first hour of immersion (24.4 $ng.cm^{-3}$), then declined over the next 3 h, and eventually reached a stable percentage of about 10.3 $ng.cm^{-3}$. This phenomenon appears to be related to the high adsorption potential of porosities and the hydrophobic nanofibers during the first stage of immersion and non-occupied hydroxyapatite ceramic sites during the final stage of immersion.

Keywords: Hydroxyapatite; Nanofibrous scaffold; Surface adsorption; Vitamin D_3.

1. INTRODUCTION

Vitamin D_3 (VD_3) is an essential organic compound that has a significant role in bone growth and is required in the production of collagen, absorption of calcium and phosphorus, and the regulation of the immune system [1-5]. On the other hand, the lack of VD_3 is a major health problem [6,7]. According to clinical interpretations, the adequate blood level of VD_3 is 30-36 $ng.ml^{-1}$, and above 100-150 $ng.ml^{-1}$ is considered as toxic [8].

Plenty of studies have focused on the biological properties of VD_3 and there are very few reports about colloidal and particle systems for the delivery of VD_3 [9,10]. However, there have been no reports about the physiochemical behaviour of VD_3 in relation to nanoporous media such as electrospun nanofibrous scaffolds. Nanofibrous scaffolds, which are fabricated by electrospinning, have numerous applications in tissue engineering due to having a polymer-ceramic composite scaffold and a nanoporous structure [11-13]. The scientific importance of the study of VD_3 adsorption by a PA6/HA nanofibrous scaffold is explained by the critical role of VD_3 in bone growth. A balanced amount of VD_3 in the surrounding environment has a significant role in bone regeneration during long term scaffold implantation.

Hydroxyapatite (HA) is well known as a bioactive ceramic added to many artificial bone tissues and implants for orthopedic surgeries [14-16]. Not only polymer/HA composites exhibit the chemical and mechanical stability of natural bones [17,18], but also they can be designed in the form of porous materials that accelerate the circulation of essential biochemical agents such as VD_3 [19]. Given the significant chemical (e.g. stability in human body) and mechanical (e.g. tensile strength and toughness) properties of polyamides, polyamide-6 (PA6) is utilized as the polymeric base of many biocomposite scaffolds [20,21].

Adsorption can occur through different routes by physical, chemical or physiochemical reactions between adsorbent and adsorbed species [22,23]. The hydrophobicity of the surface of the adsorbent has a significant role in the adsorption of vitamins and proteins [24-26]. Hydrophilic surfaces are wetted by the surrounding environment and do not allow more amino acid molecules (e.g VD_3) to adsorb onto the scaffold [27]. HA

Corresponding Author: Hamid Esfahani Received on: 10/07/2018 Accepted on: 30/09/2019

10.1590/S1517-707620200001.0927

NPs are bound to the super hydrophobic PA6 fibers, helping achieve greater VD_3 adsorption by these nanoparticles during implantation.

The present study has evaluated a nanobiomaterial, fabricated by the electrospinning procedure, in terms of its adsorption of VD_3, which is essential for bone growth. For this purpose, PA6 and PA6/HA nanofibrous scaffolds was firstly synthesized by electrospinning and then characterized by SEM, EDS, FTIR, and WCA measurements. Finally the adsorption behaviour of VD_3 was fundamentally investigated to determine the responses of the electrospun scaffolds to VD_3 molecules.

2. MATERIALS AND METHODS

2.1 Scaffold preparation

The HA NPs were synthesized in accordance to the wet chemical precipitation method commonly described in literature [28,29]. The polymer solution was prepared by dissolving 2 and 20 wt% of HA NPs and PA6 granules (1015b UBE, M_w; 15,000 $g.mol^{-1}$) in formic acid (Sigma Aldrich, 64-18-6), respectively. The components were dispersed in solution by the application of stirring and ultrasonication for 10 min at room temperature. The homogenous solution was spun by means of electrospinning which was setup with the following conditions: 15 kV apply voltage, 0.5 ml h^{-1} feed rate and 10 cm distance. The collected fibers were dried on a flat aluminium foil and then cut to appropriate size for further investigations.

2.2 Characterization of scaffolds

The thickness of the scaffolds was measured using a micrometer and the average of 10 measurements was reported. In order to study the morphology of the electrospun scaffold, the sample was sputter coated with gold and then scanning electron microscopy (JEOL- JSM 840A SEM) was applied at an accelerating voltage of 5 kV. Further investigations were conducted with ImageJ software (ImageJ 1.38, NIH, USA) to determine the diameter of the fibers and surface porosity. The morphology and composition of HA NPs and also the elemental distribution within the PA6/HA scaffold were analysed using SEM equipped with EDS setup (model Vega\TScan-20 kV). Functional molecular groups formed in the composite scaffold were evaluated using the Fourier transform infrared (FTIR) technique (Nicolet Avatar 360 FT-IR spectrometer, 4000 cm^{-1} to 400 cm^{-1}). The hydrophobicity of the scaffolds during the first minute was studied regarding water contact angle measurement (WCA) in three different locations of the samples by using a contact angle meter (VCA Optima-AST products, Billerica, MA).

2.3 Antibacterial activity test

The antibacterial activity test of PA6 and PA6/HA scaffolds were performed in a solution contacting two kinds of bacteria in accordance to the ASTM G21-1996. The *S. aureus* (ATCC 25923) and *E. coli* (ATCC 25922) were the gram-positive and gram-negative bacteria in the solution, respectively. The samples were incubated for 24 h at 37 ˚C to evaluate their antibacterial activity.

2.4 VD_3 adsorption procedure

A 1 ml VD_3 ampoule (Cholecalciferol) containing 6.16 mg of was dissolved in 37.5 ml of deionized water by stirring at room temperature. Both sides of the PA6 and PA6/HA scaffolds (1cm×1cm) were vertically exposed to 8 ml of VD_3 solution (160 $ng.ml^{-1}$) at room temperature as shown schematically in Fig. 1. Similarly, 7 scaffolds were immersed in distinct cells in order to study the effect of soaking time on adsorption of VD_3 onto mentioned scaffolds during a period of 7 h. The quantity of adsorbed VD_3 (Q_t) on the scaffolds at any time was calculated according to the following equation [22];

$$Q_t = \frac{(C_i - C_f)V}{AT} \quad (1)$$

where C_i and C_f ($mg.ml^{-1}$) are the initial and remaining concentration of VD_3 in solution, respectively. V (ml) is volume of the VD_3 solution, A (cm^2) and T (cm) stand for area and thickness of scaffolds respectively. The remaining concentration of VD_3 in solution was calculated using Beer's law [30]. For this purpose, the adsorption intensity of the surrounding solution was measured by a UV-VIS instrument (model: Cary, 100 Cone) and C_f was calculated according to the calibration curve.

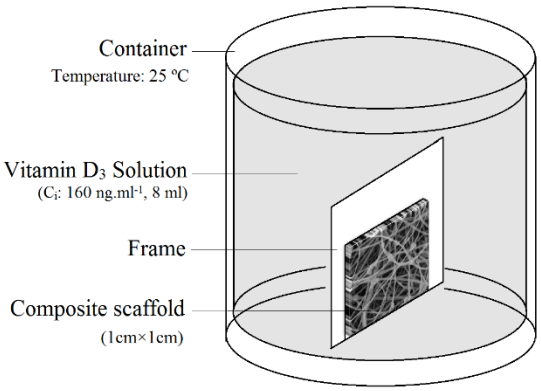

Figure 1: Set-up of VD_3 adsorption test.

3. RESULTS

3.1 Characterization of the scaffold

Prior to the fabrication of scaffolds, the synthesized HA powder was characterized regard to the morphology and composition. Fig.2 a and b present the SEM micrograph and EDS spectrum of HA powder, respectively. As can be seen, the semi-spherical particles with average size of 25.2 ± 3 nm were obtained via wet chemical precipitation method. These specifications are appropriate for blending in electrospun solution. The Ca/P ratio in HA NPs was also calculated based on the EDS spectrum, and it was found that mentioned ratio was 1.62 indicating the well coincidence with theoretical value [16]. The typical morphology of the prepared PA6 and PA6/HA scaffolds are shown in Fig. 2 c and d. It is obvious that HA NPs have been incorporated in the final microstructure of the scaffold. The HA NPs have been marked by circles, demonstrating the uniform distribution of HA aggregates within the nanofibers (NFs). According to their morphology, some NPs are attached to the stems of the fibers and some NPs are precipitated together at the junction points of the fibers. The physical specifications of nanofibrous scaffolds are given in Table 1. The obtained results declare the formation of extremely high porous, two-dimensional scaffolds, which are promising for the tissue engineering and drug delivery [31]. Moreover, the different chemical composition of nanofibrous scaffolds may make the different manner in VD_3 adsorption regard to the surface properties.

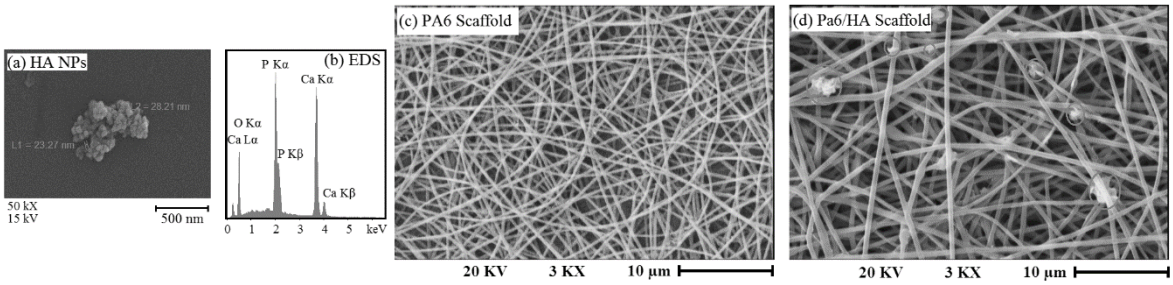

Figure 2: (a) SEM micrograph and (b) EDS of HA NPs, (c) PA6 and (d) PA6/HA SEM morphology of prepared scaffolds, the HA-NP is marked by circle.

Table 1: Physical specifications of nanofibrous scaffolds

Scaffold	Thickness of scaffold (µm)	Fibers diameter (nm)	Surface porosity (%)
PA6	120 ±10	265 ±10	74.3 ±2.3
PA6/HA	130 ±10	382 ±30	72.1 ±5.1

In addition, EDS analysis was assigned to ensure the incorporation of HA NPs into the PA6 scaffold.

The microstructure and EDS analysis of a typical area of the PA6/HA scaffold are presented in Fig. 3. The white spots in the back scattered mode SEM image are attributed to HA aggregates and the grey spots belong to the junction of PA6 NFs (see Fig. 3.a). In EDS analysis, the highest peak in the spectrum shown in Fig.3.b at 1.5 eV is attributed to the carbon (C) element which constitutes the main structure of the PA6 scaffold. The incorporation of HA particles within the nanofibrous structure was also confirmed by EDS due to the presence of Ca and P peaks at 4 and 2 eV, respectively.

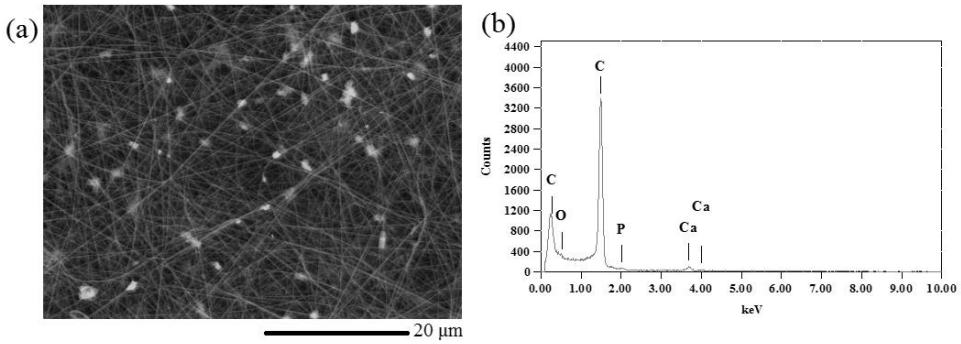

Figure 3: (a) BS-SEM image and (b) EDS analysis of typical area of PA6/HA scaffold.

In order to identify the functional molecular groups formed in the polymer/ceramic electrospun scaffold, first FTIR spectra of HA NPs and PA6 scaffold were provided as illustrations in Fig.4, and then those were compared with FTIR spectrum of PA6/HA scaffold. The prominent twin peaks at 1546 and 1641 cm^{-1} demonstrate the polyamide nature of the scaffold. The N-H stretching vibration bond of PA6 was detected at 3298 cm^{-1}, and CH_2 asymmetric stretching bonds were recognized by 1265, 1368, 1460, and 2931 cm^{-1} bands. The bands at 2861 cm^{-1} and 1170 cm^{-1} are attributed to stretching and wagging vibrations bond of CH_2, respectively [32]. Furthermore, characteristic bands related to the HA particles were also observed in the FTIR spectrum of PA6/HA. These included a low intensity band at 928 cm^{-1} assigned to the stretching vibration of P-O(H) and transmission bands at 582 cm^{-1} and 1075 cm^{-1} attributed to the bending and stretching vibrations of P-O bonds, respectively. The other bands, such as those transmitted at 711 and 3086 cm^{-1}, are related to the polyamide nature of the matrix [33]. Therefore, based on the experimental data from SEM, EDS and FTIR, it can be elucidated that HA NPs were incorporated inside of the PA6 NFs matrix without the creation of any new bonds.

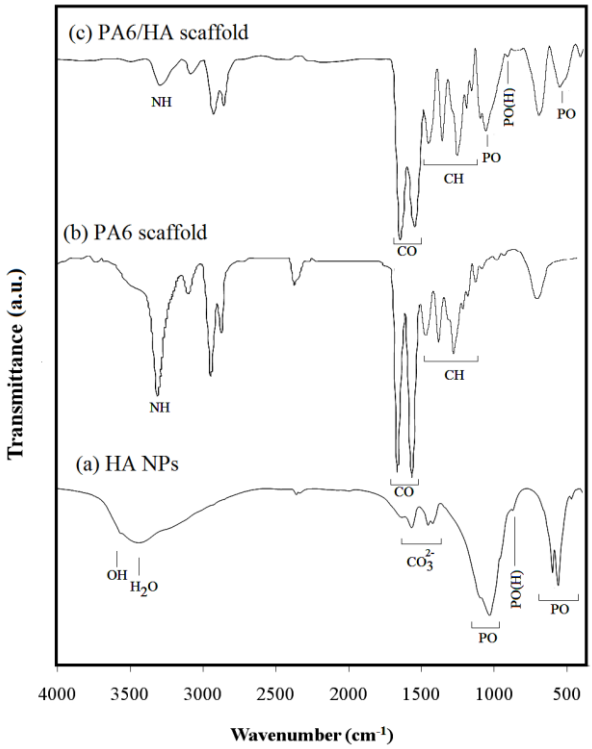

Figure 4: FTIR spectrum of (a) HA NPs, (b) PA6 and (c) PA6/HA scaffold.

Surface hydrophobicity is one of the significant characteristics which determine the biological response of a surface by affecting the arrangement of biomolecules near to the surface. Hence, the identification of the wettability of the PA6/HA scaffold by means of WCA measurement was very important for understanding its behaviour during immersion in an aqueous solution of VD_3. Fig. 5 shows the variation of WCA on PA6 and PA6/HA scaffold surfaces during the first minute of contact. It is obvious that the PA6 scaffold is super hydrophobic because the average WCA during contact time was higher than 120º. In spite of HA presence, PA6/HA also depicted a hydrophobic surface. Therefore, it is hypothesized that VD_3 molecules can arrange in a stable manner near the hydrophobic surface of the PA6/HA scaffold at preliminary time of adsorption test. This phenomenon allows the molecules to adsorb onto the surface in favourable conditions [34]. However, the WCA on PA6/HA scaffold decreased over one minute due to the unstable surface tension forces between liquid, solid and gas phases (water, scaffold and air respectively) [35].

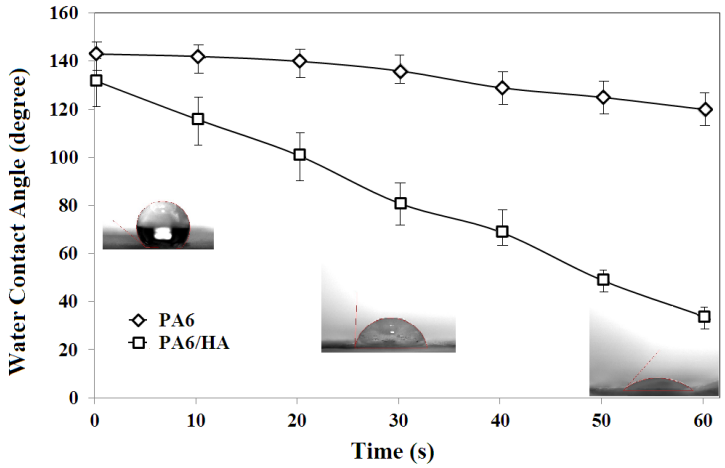

Figure 5: Variation of WCA on PA6 and PA6/HA scaffold surfaces during the first minute of contact.

3.2 Antibacterial activity

With developing the advanced materials in biomedical application, the antibacterial property of introduced material has been drawn to attention. The assessment results of the antibacterial activity of PA6 and PA6/HA scaffolds against *E. coli* and *S. aureus* showed that both scaffolds have no activity against both *E. coli* and *S. aureus* bacteria. There are many studies which have demonstrated that PA6 does not exhibit antibacterial activity [36,37]. The HA incorporation inside the PA6 NFs did not influence the antibacterial activity of PA6. The neutralized HA NPs have not interacted with the walls of the gram negative and positive bacteria [38].

3.3 Vitamin D_3 Adsorption

Due to the upper limit of VD_3 in the human body and the importance of its values in aqueous solution, the concentration variation of VD_3 in the range of adequate to toxic values was examined according to Beer's law. Fig. 6.a shows the UV spectra of VD_3 solutions with different concentrations within the mentioned range. It shows an absorbance peak at 257 nm, revealing the VD_3 variation in different concentrations from 20 to 160 $ng.ml^{-1}$. As shown in Fig. 6.b, the calibration curve was plotted with respect to the aforementioned amounts in order to generate an appropriate linear equation. Experimental data have good correspondence with the line predicted from Beer's law, demonstrating the validity of the data from the examination of VD_3 adsorption. Furthermore, the large correlation coefficient (R^2= 0.9836) demonstrated the appropriate dissolution of VD_3 in solvent and the production of a homogenous aqueous solution.

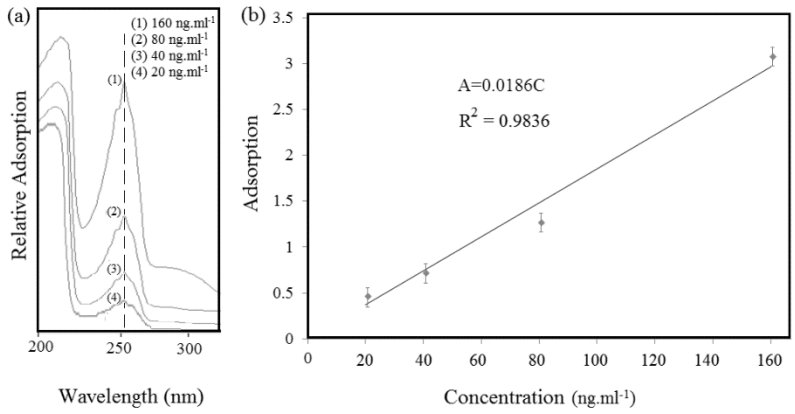

Figure 6: (a) UV spectra of VD_3 solution with different concentration, (b) calibration curve in range between 20 to 160 $ng.ml^{-1}$.

The response of the PA6 and PA6/HA scaffolds to VD_3 adsorption over a 7 h period was evaluated by Q_t index given in Eq. 1. Fig. 7 shows the variation of Q_t versus the immersion time. The variation of Q_t display the rather constant amount adsorbed by PA6 scaffold which was about 5 $ng.cm^{-3}$. In contrast, the results showed that the PA6/HA scaffold adsorbed VD_3 molecules with high efficiency over the first hour of immersion. The amount of adsorbed VD_3 declined from 24.4 to 8.3 $ng.cm^{-3}$ during the period of 1 to 4 h. Finally, adsorption efficiency improved partially and then remained constant during the period of 4 to 7 h. The final recorded amount for adsorbed VD_3 onto PA6/HA scaffold was 10.3 $ng.cm^{-3}$. Therefore, it was found that the HA NPs improve the adsorption efficiency, and three distinct stages can be assumed for adsorption: stage I: adsorption, stage II: desorption, and stage III: stability.

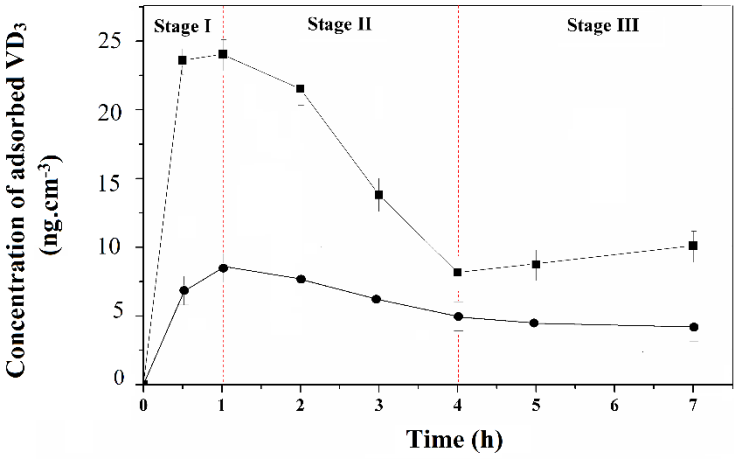

Figure 7: Amount of adsorbed VD_3 on PA6 and PA6/HA scaffolds, in period of 7 h.

The micrographs pertaining to the adsorption test of the VD_3 on PA6/HA scaffold is presented in Fig. 8. A high porous scaffold with interconnected and open porosities was observed in the sample at the starting point of the test (Fig. 8.a). This appearance dramatically changed only 0.5 h after immersion in VD_3 solution. As it can be seen in Fig. 8.b, not only the surface porosities were blocked by VD_3 molecules but also the fibers were covered by a thin layer of VD_3. Extreme adsorption also occurred for the sample which was immersed for 2 h (see Fig. 8.c). These observations are in strong agreement with results obtained by Q_t calculations. The maximum adsorption was recorded after 1 h immersion, relating to the end of stage I. More micrographs showed that blocked porosities were reopened over time, indicating the release of VD_3 into the surrounding solution. The increase in open porosities and the removal of VD_3 from NFs are demonstrated from the micrographs of the sample immersed from 2 to 4 h. This behaviour coincides with stage II and can be recognized in the area shown in Fig. 7. A similar behaviour was also observed for the immersed sample at 5 h. It is worth mentioning that the amount of adsorbed VD_3 by the last two samples was rather similar. Eventually, a rather blocked porous scaffold was observed throughout the final stage. The related micrograph may predict the long-term appearance of a PA6/HA scaffold implantation.

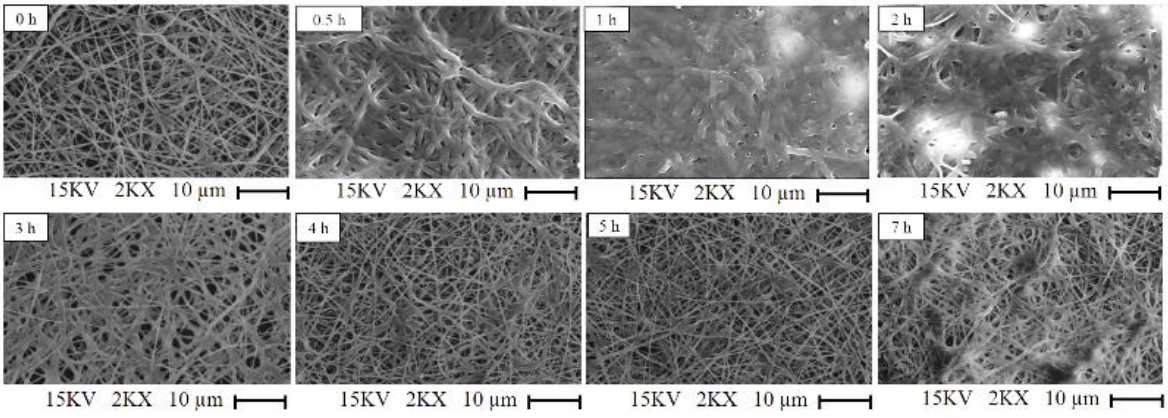

Figure 8: SEM micrographs of PA6/HA scaffold regarding to different times of immersion in VD_3 solution.

It seems that during stage I, VD_3 suddenly made a concentration gradient to adsorb on an extremely large surface area of the nanofibrous scaffolds. This rapid adsorption occurred due to the high amount of open pores at surface of scaffolds, as well as the super hydrophobic nature of the adsorbent. However, incorporation of HA NPs could intensify the adsorption efficiency of PA6 scaffold three of times. Afterwards, the main reason for the release of VD_3 from the scaffolds during stage II was the wetting of the surface after 1 h of immersion. This phenomenon resulted in repulsing VD_3, and thus the amount of adsorbed VD_3 decreased rapidly. This is in strong agreement with results reported in other research which describe that the wettability of polymeric substances is increased by the addition of amino acid species such as proteins and vitamins

[5,31]. It is worth mentioning that hydrophilic HA sites could promote the wettability of scaffold too. During stage III, HA sites of scaffolds had significant roles in holding VD_3. This is proven by the rather uniform distribution of adsorbed VD_3 on the scaffold surface as observed in the micrograph shown in Fig. 8 related to the sample at 7 h. Moreover, the amount of adsorbed VD_3 did not change perceptibly because the HA sites were occupied by the previously adsorbed VD_3. Finally, an equilibrium gradient was established between the solution and scaffold resulting in a scaffold with an area occupied by VD_3 for osteoblast progress, and open porous media for necessary biological interactions [39].

4. CONCLUSIONS

The goal of this study was to explore the adsorption behaviour of VD_3 onto electrospun nanofibrous PA6 scaffolds decorated by HA NPs. The SEM micrographs of the scaffold showed a relatively homogenous distribution of HA particles within the PA6 NFs. The average diameter size of fibers and surface porosity of PA6/HA scaffold were 213±30 nm 72.1 ± 5.1 %, respectively. EDS analysis of the PA6/HA scaffold confirmed the presence of HA particles within the fibers, and FTIR spectrum also depicted the incorporation of HA particles within the PA6 matrix, while new bonds were not formed between polymer fibers and ceramic particles. The variation of WCA during one minute signified the hydrophobic nature of the PA6/HA scaffold, helping the scaffold to adsorb more vitamin molecules. The variation of Q_t showed that the adsorption of VD_3 occurred in three stages: (I) adsorption, (II) desorption, and (III) stability. Experimental data showed that amount of adsorbedVD_3 molecules onto the PA6 and PA6/HA scaffolds was about 8.1 and 24.4 $ng.cm^{-3}$ over the first hour of immersion, and eventually reaching a stable amount of about 5 and 10.3 $ng.cm^{-3}$ respectively, which depicts the significant role of HA NPs in VD_3 adsorption. The morphology study of the PA6/HA scaffold at different times of immersion indicated dramatic changes in fibre thickness and blocked porosities after 1 h of immersion. However, an open porous media with fibers occupied by VD_3 persisted after 7 h of immersion. With the results obtained from the evaluation of VD_3 adsorption by a PA6/HA scaffold, the opportunity of creating totally controlled conditions for bone regeneration within implantations arises.

5. BIBLIOGRAPHY

[1] LUCA, H.F., "Overview of general physiologic features and functions of vitamin D", *Am J Clin Nutr*., v.80, n.6, pp. 1689-96, 2004.

[2] CHEN, L.R., WEN, Y.T., KUO, C.L., *et al*., Calcium and Vitamin D Supplementation on Bone Health: Current Evidence and Recommendations, *Int. J. Gerontol*., v.8, pp. 183-188, 2014.

[3] LI, W., PENG, H., NING, F., *et al*., "Amphiphilic chitosan derivative-based core–shell micelles: Synthesis, characterisation and properties for sustained release of Vitamin D3", *Food Chem.*, v.152, pp.307–315, 2014.

[4] CIOBANU, G., CIOBANU, O., "Investigation on the effect of collagen and vitamins on biomimetic hydroxyapatite coating formation on titanium surfaces", *Mat. Sci. Eng. C*,, v.33, pp. 1683–1688, 2013.

[5] RENO, F., AINA, V., GATTI, S., *et al*., Effect of vitamin E addition to poly (D,L)-lactic acid on surface properties and osteoblast behavior, *Biomaterials*, v.26, pp.5594–5599, 2005.

[6] SMITH, L. M., GALLAGHER, J. C., "Dietary Vitamin D Intake for the Elderly Population: Update on the Recommended Dietary Allowance forVitamin D", *Endocrin. Metab. Clin.*, v.46, n.4, pp. 871-884, 2017.

[7] BIKLE, D. D., "Vitamin D Metabolism, Mechanism of Action, and Clinical Applications", *Chem. Biol.*, v.21, n.3, pp. 319–329, 2014.

[8] REBOUCAS, P. C., NETINHO, J. G., CUNRATH, G.S., *et al*., "Hypovitaminosis D in patients with Crohn's disease", *j coloproctol*, v.36, n.2, pp. 59–63, 2016.

[9] LIN, Y., WANG, Y.H., YANG, X.Q., *et al*., "Corn protein hydrolysate as a novel nano-vehicle: Enhanced physicochemical stability and in vitro bioaccessibility of vitamin D_3", LWT – *Food. Sci. Technol. Int.*, 72 , pp. 510-517, 2016.

[10] ABBASI, A., EMAM-DJOMEH, Z., MOUSAVI, D., *et al*, "Stability of vitamin D(3) encapsulated in nanoparticles of whey protein isolate", *Food Chem.*, v.143, n.15, pp. 379-383, 2014.

[11] BENINI, K. C. C. C., CIOFFI, M. O. H., VOORWALD, H. J. C., "PHBV/cellulose nanofibrils composites obtained by solution casting and electrospinning process", *Matéria (Rio J.)*, v.22, n.2, pp.1517-7076, 2017.

[12] SANTOS, I. M. G., SANTOS, D. O., CESTARI, A. R., *et al*., "New cement slurry modified with chitosan/alginate interpenetrating networks and hydroxyapatite - structural characteristics after long-term contact with hyper-saline produced water from oil well operations", *Matéria (Rio J.)*, v.22, n.1, pp. 1517-7076, 2017.

[13] CHAO, S., LI, Y., ZHAO, R., *et al*., "Synthesis and characterization of tigecycline-loaded sericin/poly(vinyl alcohol) composite fibers via electrospinning as antibacterial wound dressings", *J Drug Deliv Sci Tec*., v.44, pp. 440-447, 2018.

[14] BARANDEHFARD, F., KIANPOUR RAD, M., HOSSEINNIA, A., *et al*., "The addition of synthesized hydroxyapatite and fluorapatite nanoparticles to a glass-ionomer cement for dental restoration and its effects on mechanical properties", *Ceram. Int*., v.42, pp. 17866–17875, 2016.

[15] WANG, Y., YANG, X., GU, Z., "In vitro study on the degradation of lithium-doped hydroxyapatite for bone tissue engineering scaffold", *Mat. Sci. Eng. C*, v. 66, pp. 185–192, 2016.

[16] EILBAGI, M., EMADI, R., RAEISSI, K., *et al*., "Mechanical and cytotoxicity evaluation of nanostructured hydroxyapatite-bredigite scaffolds for bone regeneration", *Materials Science and Engineering C*, v. 68, pp. 603–612, 2016.

[17] MACHA, I. J., NISSAN, B.B., SANTOS, J., *et al*., Biocompatibility of a new biodegradable polymer-hydroxyapatite composite for biomedical applications, *J Drug Deliv Sci Tec.*, v. 38, pp. 72-77, 2017.

[18] DIAS, J.R., GRANJA, P.L., BÁRTOLOM, P.J., "Advances in electrospun skin substitutes", *Prog. Mater. Sci.*, 84, pp. 314–334, 2016.

[19] XU, J.W., WANG, Y., YANG, Y.F., *et al*, "Effects of quaternization on the morphological stability and antibacterial activity of electrospun poly(DMAEMA-co-AMA) nanofibers", *Colloid Surfaces B: Biointerfaces*, v.133, pp. 148–155, 2015.

[20] DING, Y., HOU, H., ZHAO, Y., *et al*., "Electrospun polyimide nanofibers and their applications", *Prog. Polym. Sci.*, v.61, pp. 67–103, 2016.

[21] NOZERET, K., BONAN, M., YARMOLUK, S. M., *et al*., "Boutorine, Synthesis of mouse centromere-targeted polyamides and physico-chemical studies of their interaction with the target double-stranded DNA, *Bioorgan*", *Med. Chem.*, 23, pp. 5932–5945, 2015.

[22] ESFAHANI, H., PRABHAKARAN, M. P., SALAHI, E., *et al*., "Protein adsorption on electrospun zinc doped hydroxyapatite containing nylon 6 membrane: Kinetics and isotherm", *J. Coll. Inter. Sci*., v.443, pp. 143–152, 2015.

[23] BAKAEV, V. A., CHELNOKOVA, O. V. "Molecular theory of physical adsorption on heterogeneous surfaces: temperature dependence of henry constant", *Surf. Sci.*, v.215, pp.521-534, 1989.

[24] LOURENÇO, B. N., MARCHIOLI, G., SONG, W., *et al*., "Wettability Influences Cell Behavior on Superhydrophobic Surfaces with Different Topographies", *Biointerphases*, v.7, n.1, pp.7-46, 2012.

[25] SUN, S., YUE, Y., HUANG, X., "Deying Meng, Protein adsorption on blood-contact membranes", *J. Membrane Sci.*, v. 222, pp. 3–18, 2003.

[26] ZHAO, C., XUE, J., RAN, F., "Modification of polyethersulfone membranes – A review of methods", *Prog. Mater. Sci.*, v. 58, pp. 76–150, 2013.

[27] MATTHIASSON, E., "The role of macromolecular adsorption in fouling of ultrafiltration membranes", *J. Membrane Sci*, v. 16, pp. 23-36, 1983.

[28] ESFAHANI, H., SALAHI, E., TAYEBIFARD, A., *et al*., "Structural and morphological analysis of zinc incorporated non-stoichiometric hydroxyapatite nano powders", *Matéria (Rio J.)*, 11726, pp. 569-576, 2016.

[29] MIYAJI, F., KONO, Y., SUYAMA, Y., "Formation and structure of zinc-substituted calcium hydroxyapatite", *Mater. Res. Bull.*, v. 40, pp. 209–220, 2005.

[30] SKOOG, D.A., HOLLER, F.J., NIEMAN, T.A., *Principle of instrumental analysis*, 5th edn, Belmont, CA, Thomson Learning (1998).

[31] AQEEL BHUTTO, M., WU, T., SUN, B., *et al*., "Fabrication and characterization of vitamin B5 loaded poly(l-lactide-co-aprolactone)/silk fiber aligned electrospun nanofibers for schwann cell proliferation", *Colloid Surfaces B: Biointerfaces*, v. 144, pp. 108–117, 2016.

[32] ABDAL-HAY, A., OH, Y.S., YOUSEF, A., *et al*., "In vitro Deposition of Ca-P nanoparticles on air jet spinning nylon 6 nanofibers scaffold for bone tissue engineering", *App. Surf. Sci*. v. 307, pp.69–76, 2014.

[33] JOSHI, M. K., TIWARI, A. P., MAHARJAN, B., *et al*., "Cellulose reinforced nylon-6 nanofibrous membrane: Fabrication strategies, physicochemical characterizations, wicking properties and biomimetic mineralization", *Carbohyd. Polym.*, v.147, pp. 104–113, 2016.

[34] SUPOVA, M., "Problem of hydroxyapatite dispersion in polymer matrices: a review", *J Mater Sci: Mater Med*, 20, pp. 1201–1213, 2009.

[35] JONES, K.L., O'MELIA, CH.R. "Protein and humic acid adsorption onto hydrophilic membrane surfaces: effects of pH and ionic strength", *J. Membrane. Sci*., v. 165, pp. 31–46, 2000.

[36] SADEGHI-KIAKHANI, M., SAFAPOUR, S., "Improvement of dyeing and antimicrobial properties of nylon fabrics modified using chitosan-poly(propylene imine) dendreimer hybrid", *J. Ind. Eng. Chem*., v.33, pp.170–177, 2016.

[37] MONTAZER, M., KOMEILY NIA, Z., "Conductive nylon fabric through in situ synthesis of nanosilver: Preparation and characterization", *Mater. Sci. Eng. C*, v. 56, pp. 341–347, 2015.

[38] MA, Y., ZHOU, T., ZHAO, CH., "Preparation of chitosan–nylon-6 blended membranes containing silver ions as antibacterial materials", *Carbohyd. Res.*, v.343, pp. 230–237, 2008.

[39] LAIVA, A. L., VENUGOPAL, J. R., SRIDHAR, S., *et al*., "Novel and simple methodology to fabricate porous and buckled fibrous structures for biomedical applications", *Polymer*, v. 55, pp. 5837-5842, 2014.

ORCID

Hamid Esfahani https://orcid.org/0000-0003-1246-733X
Yasaman Ghiyasi https://orcid.org/0000-0001-5779-2553